Comput. Methods Appl. Mech. Engrg. 198 (2008) 602–613

Contents lists available at ScienceDirect

Comput. Methods Appl. Mech. Engrg.

journal homepage: www.elsevier.com/locate/cma

FE^2 computational homogenization for the thermo-mechanical analysis of heterogeneous solids

I. Özdemir, W.A.M. Brekelmans, M.G.D. Geers *

Department of Mechanical Engineering, Eindhoven University of Technology, P.O. Box 513, 5600 MB Eindhoven, The Netherlands

ARTICLE INFO

Article history:
Received 30 January 2008
Received in revised form 15 September 2008
Accepted 16 September 2008
Available online 24 September 2008

Keywords:
Multi-scale analysis
Computational homogenization
FE^2
Coarse graining
Thermo-mechanics
Heterogeneous solids

ABSTRACT

This paper presents a two-scale thermo-mechanical analysis framework for heterogeneous solids based on a computational homogenization technique. The evolution of the mechanical and thermal fields at the macroscopic level is resolved through the incorporation of the microstructural response. Within the proposed multi-scale approach, the temperature dependent non-linear thermo-mechanical response is accounted by solving a boundary value problem at the micro-scale, the results of which are properly averaged and transferred to the macro level in a consistent way. The framework does not require explicitly determined homogenized material properties (e.g. macroscopic thermal expansion coefficients) since no constitutive equations are required for the macroscopic stresses and heat fluxes at the macro level. A nested finite element solution procedure with an operator-split implementation is outlined and the effectiveness of the approach is demonstrated by illustrative key examples.

1. Introduction

In a wide spectrum of engineering structures and assemblies, premature failure of components is frequently due to severe thermal loading conditions in the form of rapid temperature changes (thermal shocks) and temperature cycles. Variations of the operating temperature of a material is mostly accompanied by physical and geometrical changes at some scale. In heterogeneous systems, local thermal expansion mismatches and thermal anisotropy of different constituents naturally triggers the appearance of internal stresses. Under highly transient external thermal loading conditions, the resulting heterogeneous temperature distribution may lead to a complicated mechanical response and a non-uniform mechanical and physical property degradation accompanied by irreversible geometrical changes. The altered distribution of mechanical properties dictates the macroscopic response as the external mechanical loading is further varied as well. Therefore, a strong coupling between the evolving microstructure and the macroscopic response arises. Moreover, microstructural configurational changes may trigger a significant interaction between the mechanical and thermal fields, for instance, in the form of a reduced heat transfer across a damaged interface. Due to the aforementioned complications, the thermo-mechanical analysis of heterogeneous material systems constitutes a challenging task.

Numerous homogenization techniques have been developed to predict the effective mechanical and thermophysical properties of materials with complex microstructures. Early research work [1,2] resulted in bounds for the effective material properties which are particularly suitable for relatively simple geometries and a restricted class of constitutive models for the phases. More general asymptotic homogenization approaches were exploited for the determination of the mechanical and thermal constitutive tensors of composites with a periodic microstructure. Starting with the work of Guedes and Kikuchi [3], the use of computational techniques within the homogenization theory has received considerable attention including applications to other field problems [4–7]. Recently the focus has shifted to extend the theory and solution algorithms to the non-linear and inelastic range [8–10]. A sub-class of computational homogenization techniques which addresses both the influence of the microstructure and the coupling with the resulting macroscopic response is presented in [11–15]. In this multi-scale approach, the macroscopic material response is obtained from the underlying microstructure by solving a boundary value problem defined on a representative volume element (RVE) of the material. The detailed treatment with underlying principles is described in [16]. At present, this method has been applied successfully for (I) stress and structural damage analysis [13,15,17], (II) the mechanical analysis of structured thin sheets (shells) [18], (III) failure analysis of cohesive interfaces [19] and (IV) heat conduction analysis in heterogenous solids [20]. In the present paper, the multi-scale framework is extended

* Corresponding author. Tel.: +31 40 247 5076; fax: +31 40 244 7355.
E-mail address: M.G.D.Geers@tue.nl (M.G.D. Geers).

0045-7825/$ - see front matter © 2008 Elsevier B.V. All rights reserved.
doi:10.1016/j.cma.2008.09.008

to the fully coupled thermo-mechanical analysis of heterogeneous material systems including an appropriate solution algorithm.

The interaction of the thermal and mechanical fields within a multi-scale modeling framework requires comprehensive treatment and depends on the characteristic micro-failure mechanisms. For typical high temperature resistant materials (e.g. refractory ceramics), micro-failure mechanisms such as debonding of the grain–grain interfaces, evolve at an apparent microstructural level, which motivates a two-level treatment as adopted in the following sections. Furthermore, damage and failure at the micro level takes place without significant inelasticity (e.g. plasticity), which implies that the effect of mechanical energy dissipation on the thermal field is negligible and therefore not taken into account in the analysis. Similarly, the reduction of the heat flow as a result of mechanical damage is not explicitly considered although the constructed framework can easily accommodate such coupling effects. Before proceeding further, the essential points on which the proposed framework differs from the existing approaches can be summarized as:

- The proposed approach does not require macroscopic material properties such as the homogenized coefficient of thermal expansion as opposed to other alternative homogenization schemes.
- The framework has the flexibility to include a non-linear and temperature dependent thermo-mechanical material response at the microstructural level, which is transmitted to the macro level in a consistent way. Furthermore, for different combinations and types of constitutive equations at the micro level, re-derivation of certain effective quantities (expressions) is not necessary.
- The presented solution algorithm resolves the interaction of the fields in a proper way and can accommodate thermo-mechanically induced coupling mechanisms accompanying microstructural evolution.

The presentation of the paper is organized as follows. After the introduction of the assumptions in the next section, the thermo-mechanical analysis problems at micro and macro levels are formulated in Section 3. Then, the scale transition structure is summarized in Section 4. Thereupon, a two-scale solution strategy is presented which leads to an operator-split nested finite element solution algorithm further detailed in Section 5. Illustrative examples are presented in Section 6, followed by the discussion and conclusion section.

2. Preliminaries

In this paper, a first order theory is adopted for both the mechanical and thermal homogenization procedure which hinges on the principle of scale separation [13,15,20]. A first order theory for mechanical homogenization implies that the macroscopic deformation gradient varies mildly and therefore deformation localization (softening) is excluded from the considerations. However, for typical high temperature resistant structures, the onset of softening is practically the end of service life (failure) since after the onset the bearing capacity is very limited. Theoretically, the principle of scale separation assumes an infinitesimally small underlying fine scale structure (infinitesimal neighbourhood of a material point) though finite sized RVE's are used in real predictive computations. As a matter of fact, a steady-state temperature profile is assumed at the micro level in virtue of the negligibly small size of the RVE. In fact, what is meant by 'steady-state' is 'instantaneous temperature changes' at the micro level which are dictated through the boundary conditions as discussed in Section 4.1.

As will be clarified in Section 5, the RVE analysis is performed to extract macroscopic stresses, heat fluxes and associated tangent operators. Therefore, the RVE analysis can be partly considered as a substitute for the so-called 'algorithmic stress update boxes' (stress integration algorithms) derived from phenomenological models for which the body forces and heat sources are irrelevant [21]. Furthermore, for stationary mechanical loading, inertia effects are neglected.

3. Micro- and macro-scale problem formulations

3.1. Micro-scale problem

The evolution of thermal and mechanical fields at the micro level is defined and monitored on a representative volume element (RVE) provided with the essential physical and geometrical information about the microstructural components. Particularly for materials with random microstructures, the choice of the RVE is a delicate task. The difficulty arises due to the fact that RVE should be statistically representative of all microstructural heterogeneities and at the same time remain small enough so that the principle of scale separation is not violated. Furthermore, the RVE response should be independent of the applied boundary conditions. A detailed discussion and relevant techniques to determine the RVE size is given in [22,23] and the references therein. Here, it is assumed that an appropriate RVE has already been selected. In Fig. 1, the reference and current configuration of a microstructured 2-D domain is shown where the subscript '0' is used for referential quantities. For a particular material point P, the underlying 2-D initially square RVE is depicted in both configurations, for which V and Γ are the current volume and boundary of the micro-domain, respectively. The RVE boundary is further split up into Γ^L for the left side of the boundary, Γ^R for the right, etc. The thermal and mechanical characterizations of the phases at the RVE level are described by their respective constitutive relations. Note that there are no a priori restrictions on the specification of the constitutive laws and material parameters (e.g. temperature dependent, anisotropic, etc.) other than the fundamental thermodynamical limitations.

In a geometrically non-linear setting, in the absence of body forces and inertia effects, the mechanical equilibrium at the micro-domain takes the form,

$$\vec{\nabla}_{\mathrm{m}} \cdot \boldsymbol{\sigma}_{\mathrm{m}} = \vec{0}, \tag{1}$$

in which $\boldsymbol{\sigma}_{\mathrm{m}}$ is the microscopic Cauchy stress tensor defined by the corresponding constitutive law whose description might be anisotropic and depending on the temperature and a set of internal variables. In (1), $\vec{\nabla}_{\mathrm{m}}$ indicates the gradient operator with respect to the current micro-domain. The mechanical RVE problem is complemented with standard boundary conditions, for which periodic boundary conditions provide the best approximation [24]. Based on the assumptions introduced in Section 2, the steady-state heat balance at the micro level is expressed as,

$$\vec{\nabla}_{\mathrm{m}} \cdot \vec{q}_{\mathrm{m}} = 0, \tag{2}$$

where $\vec{q}_{\mathrm{m}}$ is the microscopic heat flux vector. To construct a well-posed problem, the balance equation is to be complemented with the temperature and heat flux boundary conditions. The specific form of the boundary conditions will be outlined in Section 4.

3.2. Macro-scale problem

At the macro level, the mechanical equilibrium has an identical structure as at the micro level

$$\vec{\nabla}_{\mathrm{M}} \cdot \boldsymbol{\sigma}_{\mathrm{M}} = \vec{0}, \tag{3}$$

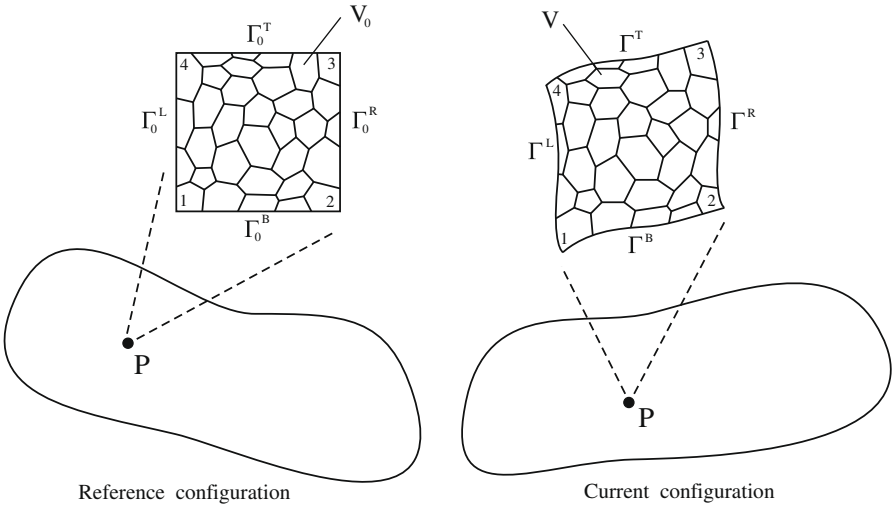

Fig. 1. Macroscopic and microstructural domain.

which is complemented by the macroscopic mechanical boundary conditions. In the absence of heat sources, the conservation of thermal energy equation at the macro level takes the general time dependent form according to

$$(\rho c_v)_{\mathrm{M}}\dot{\theta}_{\mathrm{M}} + \vec{\nabla}_{\mathrm{M}} \cdot \vec{q}_{\mathrm{M}} = 0, \tag{4}$$

where θ_{M}, $\vec{q}_{\mathrm{M}}$ and $(\rho c_v)_{\mathrm{M}}$ represent the temperature, the heat flux and the heat storage capacity, respectively. In addition to proper thermal boundary conditions, also initial conditions have to be specified for the temperature distribution at the macro level.

Within the proposed computational homogenization procedure, the macroscopic Cauchy stress and the macroscopic heat flux are obtained from the solution of the micro-scale thermo-mechanical problem defined on the underlying microstructure (RVE). In addition to these flux quantities, the discretized weak forms of the macroscopic governing equations require the macroscopic (tangent) conductivity, the macroscopic mechanical tangent stiffness and the macroscopic heat storage capacity $(\rho c_v)_{\mathrm{M}}$ to enable the solution of the resulting system of equations. Consistent derivations of these macroscopic quantities are elaborated in the following sections.

4. Scale transitions

4.1. The macro–micro scale transition

Within the framework of a first order multi-scale analysis, the actual microscopic displacement and temperature fields at a location $\vec{x}$ in the current configuration can be decomposed without loss of generality as

$$\vec{u}_{\mathrm{m}}(\vec{x}) = (\boldsymbol{F}_{\mathrm{M}} - \boldsymbol{I}) \cdot (\vec{X} - \vec{X}_1) + \vec{u}_{\mathrm{f}}(\vec{x}), \tag{5a}$$

$$\theta_{\mathrm{m}}(\vec{x}) = \theta^{\mathrm{r}}_{\mathrm{m}} + \vec{\nabla}_{\mathrm{M}}\theta_{\mathrm{M}} \cdot (\vec{x} - \vec{x}_1) + \theta_{\mathrm{f}}(\vec{x}) \tag{5b}$$

in a macroscopic contribution and a fluctuation field (subscript 'f') that represents the fine scale deviations with respect to the average fields as a result of the variations in material properties within the RVE. In Eqs. (5), the displacement $\vec{u}_{\mathrm{m}}$ and the temperature θ_{m} are presented with respect to the corresponding values of corner 1. In Eq. (5a), $\vec{X}$ denotes the position vector in the reference configuration, whereas in Eq. (5b) the current position vector, $\vec{x}$, is used implying that two different configurations are involved for the decomposition of displacement and temperature fields, respectively. For Eq. (5a), although other referential or spatial kinematic quantities could be used, the description in terms of $\boldsymbol{F}_{\mathrm{M}}$ and referential position vectors leads to compact scale transition relations, [16]. For the decomposition (5b), a formulation based on the current configuration is preferred since a fully referential description requires pull-back of the primary quantities (temperature gradient and heat fluxes) leading to more complicated scale bridging relations. To suppress the rigid body translation, corner 1 is taken to be fixed, $\vec{u}_{\mathrm{f}}(\vec{x}_1) = \vec{0}$, whereas the rigid body rotation is excluded by the periodic displacement constraint introduced further on. However, fixing the temperature level for the RVE is less trivial. The temperature profile at the micro level results from the imposed boundary conditions and the distinct conductivities of the microstructural phases, which may be temperature dependent. Therefore, the determination of the reference temperature in the micro-domain which has been indicated by $\theta^{\mathrm{r}}_{\mathrm{m}}$ is required for a reliable solution. To this end, an additional constraint,

$$(\rho c_v)_{\mathrm{M}}\theta_{\mathrm{M}} = \frac{1}{V}\int_V (\rho c_v)_{\mathrm{m}}\theta_{\mathrm{m}}\,\mathrm{d}V \tag{6}$$

is proposed. This condition is sufficient to obtain a unique temperature profile and enforces a temperature distribution that respects the consistency of the stored heat at micro and macro level.

In computational homogenization, the macro-to-micro transition is achieved by enforcing the conditions,

$$\boldsymbol{F}_{\mathrm{M}} = \frac{1}{V_0}\int_{V_0} \boldsymbol{F}_{\mathrm{m}}\,\mathrm{d}V_0, \tag{7a}$$

$$\vec{\nabla}_{\mathrm{M}}\theta_{\mathrm{M}} = \frac{1}{V}\int_V \vec{\nabla}_{\mathrm{m}}\theta_{\mathrm{m}}\,\mathrm{d}V, \tag{7b}$$

which essentially imposes a volumetric averaging of the primary deformation characteristics ($\boldsymbol{F}$, deformation gradient) and the essential driving forces for the heat flow ($\vec{\nabla}\theta$, temperature gradient), bridging the two scales.

The substitution of Eqs. (5) into the scale transition relations Eqs. (7) leads to the conditions

$$\int_{\Gamma_0} \vec{u}_{\mathrm{f}}\,\mathrm{d}\Gamma_0 = \vec{0}, \tag{8a}$$

$$\int_{\Gamma} \theta_{\mathrm{f}}\,\mathrm{d}\Gamma = 0, \tag{8b}$$

which are the basis for different types of boundary conditions that can be imposed at the micro level. For instance, enforcing periodic fluctuation fields results in

$$\vec{u}_{\mathrm{f}}^{L} = \vec{u}_{\mathrm{f}}^{R} \rightarrow \vec{u}_R = \vec{u}_L + (\boldsymbol{F}_{\mathrm{M}} - \boldsymbol{I}) \cdot (\vec{X}_R - \vec{X}_L), \tag{9a}$$

$$\vec{u}_{\mathrm{f}}^{\mathrm{T}} = \vec{u}_{\mathrm{f}}^{B} \rightarrow \vec{u}_T = \vec{u}_B + (\boldsymbol{F}_{\mathrm{M}} - \boldsymbol{I}) \cdot (\vec{X}_T - \vec{X}_B), \tag{9b}$$

$$\theta_{\mathrm{f}}^{L} = \theta_{\mathrm{f}}^{R} \rightarrow \theta_R = \theta_L + \vec{\nabla}_{\mathrm{M}}\theta_{\mathrm{M}} \cdot (\vec{x}_R - \vec{x}_L), \tag{9c}$$

$$\theta_{\mathrm{f}}^{\mathrm{T}} = \theta_{\mathrm{f}}^{B} \rightarrow \theta_T = \theta_B + \vec{\nabla}_{\mathrm{M}}\theta_{\mathrm{M}} \cdot (\vec{x}_T - \vec{x}_B), \tag{9d}$$

which are known to yield better convergence to apparent macroscopic properties as compared to other options (e.g., fully prescribed boundary conditions: $\vec{u}_{\mathrm{f}} = \vec{0}$ and $\theta_{\mathrm{f}} = 0$ on Γ), see [24]. Periodically microfluctuating temperature boundary conditions result in non-homogenous linear relations between the temperatures of the opposite edges which are similar to the constraints arising in second order computational homogenization [25]. Therefore, the stored heat consistency condition (Eq. (6)) and the periodically microfluctuating temperature boundary conditions lead to a time-independent (instantaneous) temperature profile dictated by the macroscopic temperature, macroscopic temperature gradient and local conductivities within the RVE. However, it is important to note that the macroscopic temperature and the temperature gradient changes as the macroscopic loading is further varied. This 'instantaneous' temperature profile at the RVE directly results from the adopted principle of separation of scales, as commented in Section 2. Nevertheless, extensions towards a transient analysis at the RVE level are of course possible as presented in [26], where a transient (non-Fourier) heat conduction at the micro level is employed within the framework of an asymptotic homogenization method.

Furthermore, it is important to realize that in the absence of fluctuation terms (e.g. homogenous conductivity at the RVE level) the imposed boundary conditions reflect a linear temperature profile at the RVE level. It is worth to note that the current geometry of the RVE influences the thermo-mechanical response through the imposition of the boundary conditions in the current state, Eqs. (9c) and (9d). Furthermore, particularly in the vicinity of macroscopic Dirichlet boundary conditions, the temperature gradient can vary rapidly so that the principle of scale separation might be violated. In other words, the variation of the macroscopic temperature profile should be mild enough as compared to the RVE dimensions so that the macroscopic temperature gradient can be taken as constant over an RVE area. This is a limitation of the proposed method. Due to the different configurations employed, referential and current volume integrals are used in Eqs. (7a) and (7b) from which boundary integrals (8a) and (8b) are obtained, respectively.

4.2. The micro–macro scale transition

For the determination of the macroscopic heat storage capacity $(\rho c_v)_{\mathrm{M}}$, used in Eq. (4), the following volume averaging is proposed:

$$(\rho c_v)_{\mathrm{M}} = \frac{1}{V}\int_V (\rho c_v)_{\mathrm{m}}\,\mathrm{d}V, \tag{10}$$

which is fully in line with the equivalent result obtained through an asymptotic homogenization method [27]. This equation implies that the heat capacity is consistently preserved upon scale bridging.

The micro-to-macro transition is essentially based on two principles. The mechanical coupling hinges on the macro-homogeneity (Hill-Mandel) condition, written in terms of the work conjugate pair $\boldsymbol{F}$ (deformation gradient tensor) and $\boldsymbol{P}$ (first Piola–Kirchhoff stress tensor) as:

$$\boldsymbol{P}_{\mathrm{M}} : \delta\boldsymbol{F}_{\mathrm{M}} = \frac{1}{V_0}\int_{V_0} \boldsymbol{P}_{\mathrm{m}} : \delta\boldsymbol{F}_{\mathrm{m}}\,\mathrm{d}V_0. \tag{11}$$

The symbol ':' indicates the double contraction and for second order tensors yields, $\mathbf{A} : \mathbf{B} = A_{ij}B_{ij}$. This principle simply expresses the volumetric consistency of the macroscopic internal virtual work and that of the underlying microstructural volume.

For the thermal part, the motivation originates from the second law of thermodynamics, which requires a positive entropy change due to heat conduction. Enforcing the volumetric consistency of the micro and macro entropy increase due to heat conduction leads to,

$$\vec{\nabla}_{\mathrm{M}}\theta_{\mathrm{M}} \cdot \vec{q}_{\mathrm{M}} = \frac{1}{V}\int_V \vec{\nabla}_{\mathrm{m}}\theta_{\mathrm{m}} \cdot \vec{q}_{\mathrm{m}}\,\mathrm{d}V, \tag{12}$$

which is the basis for the micro-to-macro transition in the context of the conservation of thermal energy. Note that Eq. (12) is not exactly the entropy statement (no temperature scaling applied), but is nevertheless well motivated, see [28].

It can be shown that for each of the boundary conditions of interest, the scale bridging principles lead to [16,20],

$$\boldsymbol{P}_{\mathrm{M}} = \frac{1}{V_0}\int_{V_0} \boldsymbol{P}_{\mathrm{m}}\,\mathrm{d}V_0, \tag{13a}$$

$$\vec{q}_{\mathrm{M}} = \frac{1}{V}\int_V \vec{q}_{\mathrm{m}}\,\mathrm{d}V. \tag{13b}$$

From Eq. (13a) the macroscopic Cauchy stresses are obtained by the standard relation $\boldsymbol{\sigma}_{\mathrm{M}} = \frac{1}{\det \boldsymbol{F}_{\mathrm{M}}}\boldsymbol{P}_{\mathrm{M}} \cdot \boldsymbol{F}_{\mathrm{M}}^{\mathrm{T}}$, where $\boldsymbol{F}_{\mathrm{M}}^{\mathrm{T}}$ is the transpose of $\boldsymbol{F}_{\mathrm{M}}$.

5. Two-scale numerical solution framework

Since analytical solutions are limited to relatively simple geometries and constitutive relations, a general approximate solution procedure is pursued on the basis of the finite element method at both scales (FE^2). Both mechanical and thermal boundary conditions are parameterized in a (pseudo-)time setting and applied incrementally. Furthermore, in case of transient thermal problems, a proper numerical time integration scheme is introduced to convert the spatially discretized rate equations into a fully discrete form. Non-linear equations resulting from the mechanical and heat balances have to be solved with an incremental-iterative solution procedure. To incorporate the constitutive behaviour at the macro level, an RVE is associated to each macroscopic integration point.

The interaction between the mechanical and thermal fields through the temperature induced stresses, temperature dependent material properties and the influence of geometrical changes (large displacements and internal discontinuities) on the thermal field leads to a coupled problem at both micro and macro levels.

The implementation of the coupling between both fields is based on an operator-split approach in which two sub-problems are solved sequentially leading to two incrementally uncoupled balance equations. For this purpose, a thermal balance with an updated and frozen mechanical field is solved, followed by a mechanical equilibrium problem with an updated and frozen thermal field. The resulting numerical scheme has a simple structure with symmetric system matrices but is only conditionally stable. Since an incremental-iterative solution scheme already requires small time steps to handle the non-linearities, the operator-split approach does not necessarily involve higher computational costs.

In the following sections, the macroscopic boundary value problem (BVP) and the microscopic BVP are further elaborated within the aforementioned framework.

5.1. Macroscopic boundary value problem

As a result of geometrical and/or material non-linearities, the resulting balance equations are non-linear as well and have to be solved by a Newton–Raphson technique in an incremental-iterative way. In the current increment, at iteration k, estimates are denoted as $\underline{u}^{(k)}$ for the nodal displacements and $\underline{\theta}^{(k)}$ for the nodal temperatures, where a bar under a symbol is used to indicate

columns (representation of vectors with respect to a certain basis in matrix notation) and matrices. Upon linearization, the out of balance (residual) nodal forces and heat fluxes have to vanish, i.e.

$$\underline{r}_{\text{mech}}(\underline{u}^{(k)}) = \underline{f}_{\text{int}}(\underline{u}^{(k)}) - \underline{f}_{\text{ext}} \rightarrow \underline{r}_{\text{mech}}(\underline{u}^{(k)}) + \delta\underline{r}_{\text{mech}} = \underline{0}, \tag{14a}$$

$$\underline{r}_{\text{th}}(\underline{\theta}^{(k)}) = \underline{q}_{\text{int}}(\underline{\theta}^{(k)}) - \underline{q}_{\text{ext}} \rightarrow \underline{r}_{\text{th}}(\underline{\theta}^{(k)}) + \delta\underline{r}_{\text{th}} = \underline{0}, \tag{14b}$$

where $\delta\underline{r}_{\text{th}}$ and $\delta\underline{r}_{\text{mech}}$ are the iterative updates of the nodal heat fluxes and forces which tend to zero within the limit of the adopted convergence norm. Using an updated Lagrangian framework (whereby the current configuration is taken as the reference for volume integration [29]), the corrections $\delta\underline{r}_{\text{th}}$ and $\delta\underline{r}_{\text{mech}}$ are expressed in the nodal variations $\delta\underline{u}$ and $\delta\underline{\theta}$ as

$$\delta\underline{r}_{\text{mech}} = \sum_{e=1}^{n_{el}} \left[\int_{V^e} (\underline{B}^{\text{T}}\underline{C}_{\text{M}}\underline{B} + \underline{H}^{\text{T}}\underline{S}\underline{H}) \text{d}V \right] \delta\underline{u}, \tag{15a}$$

$$\delta\underline{r}_{\text{th}} = \sum_{e=1}^{n_{el}} \left[\int_{V^e} \left(\frac{1}{\Delta t}(\rho c_v)_{\text{M}} \underline{N}^{T}\underline{N} + \underline{B}^{\text{T}}\underline{K}_{\text{M}}\underline{B} \right) \text{d}V \right] \delta\underline{\theta}. \tag{15b}$$

A backward Euler time integration scheme is employed to construct the fully discrete system of Eqs. (15b). The key ingredients of these equation systems (Eqs. (15a) and (15b)) are the macroscopic spatial material tangent stiffness in Voigt notation $\underline{C}_{\text{M}}$, the macroscopic heat storage capacity $(\rho c_v)_{\text{M}}$ and the macroscopic tangent conductivity $\underline{K}_{\text{M}}$, respectively. In a standard manner, spatial derivatives of the shape functions are placed in matrix $\underline{B}$ and the matrix $\underline{N}$ is composed of the shape functions. Furthermore, the second term in the integrand of (15a) is the so-called initial stress component of the tangent stiffness for which $\underline{H}$ and $\underline{S}$ are defined as,

$$\underline{H} = \begin{bmatrix} N_{1,x} & 0 & N_{2,x} & 0 & \cdots \\ N_{1,y} & 0 & N_{2,y} & 0 & \cdots \\ 0 & N_{1,x} & 0 & N_{2,x} & \cdots \\ 0 & N_{1,y} & 0 & N_{2,y} & \cdots \end{bmatrix} \quad \text{and} \quad \underline{S} = \begin{bmatrix} \underline{\sigma}_{\text{M}} & \underline{0} \\ \underline{0} & \underline{\sigma}_{\text{M}} \end{bmatrix} \tag{16}$$

$$\text{with } \underline{\sigma}_{\text{M}} = \begin{bmatrix} \sigma_{11} & \sigma_{12} \\ \sigma_{21} & \sigma_{22} \end{bmatrix}$$

for a two-dimensional discretization [30], where $\underline{\sigma}_{\text{M}}$ is the macroscopic Cauchy stress matrix.

The solution algorithm for time step [t_n to t_{n+1}] is depicted in Table 1. At the macro level, each increment consists of a 'thermal pass' and a 'mechanical pass' for which the heat fluxes, stresses and relevant tangent operators are extracted from the RVE level problem. In the following sections, essential components of the multi-scale solution scheme will be explained in more detail. The high computational cost of this scheme can be reduced substantially by parallel computing. Although an implicit solution algorithm is presented here, explicit time marching which requires much smaller time steps, could be equally used. However, this would not bring considerable gain since the computational burden is on the solution of RVE level problem but not on the extraction of macroscopic tangent stiffnesses and the solution of the macroscopic systems.

It is worth to note that a staggered approach with a proper bookkeeping allows the use of different time stepping for mechanical and thermal problems. This might be particularly useful in case of Dirichlet type thermal boundary conditions at the beginning of the loading history.

5.2. RVE level boundary value problem

Essential components of the macroscopic solution procedure (fluxes and tangent operators) require the solution of the micro level BVP's for both macroscopic thermal and mechanical passes. Similar to the macro level BVP, a finite element solution procedure is adopted for the micro BVP's including the extraction of the macroscopic heat fluxes, stresses and tangent operators.

Table 1
Two-scale staggered solution scheme for the thermo-mechanical analysis

Macro		Micro
Next increment		
I. Thermal pass:		
(a) Next iteration		
▷ assemble the tangent conductivity		
▷ solve the system and update θ_{M}		
▷ loop over all integration points	$\theta_{\text{M}}, \vec{\nabla}_{\text{M}}\theta_{\text{M}} \xrightarrow{}$ RVE at t_n $\xleftarrow{} \vec{q}_M, K_M$	▷ solve the RVE problem ▷ calculate macroscopic heat flux and conductivity
▷ store $\vec{q}_{\text{M}}$ and K_M		
▷ end integration point loop		
▷ assemble the internal nodal fluxes		
▷ check for convergence, if not repeat step (a), else continue		
II. Mechanical pass:		
(b) Next iteration		
▷ assemble the tangent stiffness		
▷ solve the system and update $\mathbf{F}_{\text{M}}$		
▷ loop over all integration points	$\Delta\mathbf{F}_{\text{M}}, \theta_{\text{M}}, \vec{\nabla}_{\text{M}}\theta_{\text{M}} \xrightarrow{}$ RVE at t_n $\xleftarrow{} \boldsymbol{\sigma}_{\text{M}}, \mathbb{A}_{\text{M}}$ updated RVE state	▷ solve the RVE problem ▷ calculate the macroscopic stresses and stiffness
▷ store $\boldsymbol{\sigma}_{\text{M}}$ and $\mathbb{A}_{\text{M}}$		
▷ end integration point loop		
▷ assemble the internal forces		
▷ check for convergence, if not repeat step (b), else save updated RVE state at t_{n+1} and start new increment		

5.2.1. RVE–BVP coupled to the macroscopic thermal pass

This section is essentially based on the computational homogenization scheme introduced in [20]. Related details are therefore not given here.

On an updated micro-domain (RVE at t_n passed to micro level in the macroscopic thermal pass, see Table 1), the discretization of the weak form of the microscopic heat balance equation leads to a system of (non-)linear algebraic equations in the unknown nodal temperatures $\underline{\theta}$, which can be written as

$$\underline{q}_{\text{int}}(\underline{\theta}) = \underline{q}_{\text{ext}} \tag{17}$$

expressing that the externally applied nodal heat fluxes are equilibrated by the nodal internal fluxes. The system is excited by the macroscopic loading term $\underline{\Upsilon}_{\text{M}}$, a column consisting of the macroscopic temperature and the components of the macroscopic temperature gradient with respect to the base vectors $\vec{e}_1$, $\vec{e}_2$

$$\underline{\Upsilon}_{\text{M}} = \begin{bmatrix} \theta_{\text{M}} \\ (\vec{\nabla}_{\text{M}})_1 \\ (\vec{\nabla}_{\text{M}})_2 \end{bmatrix}, \tag{18}$$

which is imposed on the system through the periodically microfluctuating temperature boundary conditions (see Eqs. (9c) and (9d)) and the stored heat consistency condition (see Eq. (6)). In case of temperature dependent conductivities at the micro level, the equilibrium solution can be obtained iteratively using a classical Newton–Raphson scheme. To this purpose, Eq. (17) is linearized with respect to the incremental estimates $\underline{\theta}^k$, which yields the following system for the iterative corrections $\delta\underline{\theta}$

$$\underline{K}\delta\underline{\theta} = \underline{q}_{\text{ext}} - \underline{q}_{\text{int}}(\underline{\theta}^k), \tag{19}$$

where the tangent conductivity matrix $\underline{K}$ is defined by $\underline{K} = \frac{\partial \underline{q}_{\text{int}}}{\partial \underline{\theta}}\Big|_{\underline{\theta}^k}$.

In order to impose the periodically microfluctuating temperature boundary conditions, linear dependencies are introduced in the system in a classical manner. To ease the implementation, the RVE domain is discretized in such a way that the nodes on opposite sides match geometrically, see Fig. 2. The periodically microfluctuating boundary conditions applied to the edge nodes ($\underline{\theta}_e$, excluding the corner nodes) lead to a set of linear constraint equations of a non-homogeneous type which can be expressed as,

$$\underline{\theta}_e = \underline{T}\underline{\theta}_n + \underline{G}\underline{\Upsilon}_M \tag{20}$$

where $\underline{T}$ and $\underline{G}$ are the coefficient matrices of the tying relations and $\underline{\theta}_n$ is the column with the independent (master) degrees of freedom (left and bottom edges, excluding corner nodes). With the introduced transformation, the explicit form of the partitioned system of equations is given as,

$$\begin{bmatrix} \underline{T}^T\underline{K}_{ee}\underline{T} & \underline{T}^T\underline{K}_{ei} & \underline{T}^T\underline{K}_{ec} \\ \underline{K}_{ie}\underline{T} & \underline{K}_{ii} & \underline{K}_{ic} \\ \underline{K}_{ce}\underline{T} & \underline{K}_{ci} & \underline{K}_{cc} \end{bmatrix} \begin{bmatrix} \delta\underline{\theta}_n \\ \delta\underline{\theta}_i \\ \delta\underline{\theta}_c \end{bmatrix} = \begin{bmatrix} -\underline{q}_n^{\text{int}} - \underline{q}_d^{\text{int}} \\ -\underline{q}_i^{\text{int}} \\ \underline{q}_c^{\text{ext}} - \underline{q}_c^{\text{int}} \end{bmatrix}, \tag{21}$$

where $\underline{q}_n^{\text{int}}$ (independent, left and bottom edges) and $\underline{q}_d^{\text{int}}$ (dependent, right and top edges) appearing on the right-hand side are the corresponding subcolumns of the internal nodal heat flux column of edge nodes. In Eq. (21) the subscript '*i*' refers to the internal (not located on the boundaries) degrees of freedom and subscript '*c*' designates the quantities associated with corner nodes, see Fig. 2.

Further on, the periodically microfluctuating temperature boundary conditions for the corner nodes (e.g. $\theta_2 = \theta_1 + \vec{\nabla}_M\theta_M \cdot (\vec{x}_2 - \vec{x}_1)$) and the stored heat consistency condition (Eq. (6)) lead to four independent equations which can be compactly expressed in a variational (incremental or iterative) form as,

$$[\underline{M}_{ce} \quad \underline{M}_{ci} \quad \underline{M}_{cc}] \begin{bmatrix} \delta\underline{\theta}_e \\ \delta\underline{\theta}_i \\ \delta\underline{\theta}_c \end{bmatrix} = [\underline{M}_{ce}\underline{T} \quad \underline{M}_{ci} \quad \underline{M}_{cc}] \begin{bmatrix} \delta\underline{\theta}_n \\ \delta\underline{\theta}_i \\ \delta\underline{\theta}_c \end{bmatrix} = \underline{0}, \tag{22}$$

where $\underline{M}_{(ce,ci,cc)}$ are the coefficient matrices. Using these constraints, the resulting system of equations can be solved and an update for the unknown temperature column $\underline{\theta}$ is obtained [20].

5.2.2. Extraction of the macroscopic heat flux

As shown in Ref. [20], after discretization, the volume averaging relation for $\vec{q}_M$ can be expressed as

$$\vec{q}_M = \frac{1}{V}\left((\vec{x}_L - \vec{x}_R)\sum \underline{q}_L^{\text{ext}} + (\vec{x}_B - \vec{x}_T)\sum \underline{q}_B^{\text{ext}} + \underline{\vec{x}}_c^T\underline{q}_c^{\text{ext}}\right), \tag{23}$$

where $\underline{q}_L^{\text{ext}}$ and $\underline{q}_B^{\text{ext}}$ are the columns of nodal heat fluxes at the left and bottom edges, respectively. The summations are performed over the components of the corresponding columns. The last term $\underline{\vec{x}}_c\underline{q}_c^{\text{ext}}$ (with $\underline{\vec{x}}_c$, a column with corner node position vectors) represents the contribution of the heat fluxes at the corner nodes. Eq. (23) can be conveniently expressed in components using a matrix-column format as

$$\underline{q}_M = [\underline{L}_n \quad \underline{L}_c] \begin{bmatrix} \underline{q}_n^{\text{ext}} \\ \underline{q}_c^{\text{ext}} \end{bmatrix}, \tag{24}$$

where $\underline{L}_n$ and $\underline{L}_c$ are implicitly defined.

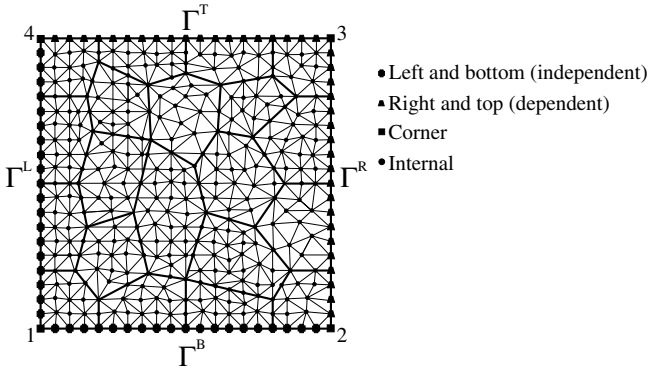

Fig. 2. Discretized RVE example.

5.2.3. Extraction of the macroscopic conductivity

To solve the macroscopic problem, a relation between the variation of the macroscopic heat flux and the variation of the macroscopic temperature gradient is required, which is written as

$$\delta\underline{q}_M = \underline{K}_M\delta(\underline{\nabla}_M\theta_M), \tag{25}$$

where $\underline{K}_M$ is the macroscopic (tangent) conductivity at integration point level of the macroscopic discretization. To this end, the variation of the macroscopic heat flux expression Eq. (24) is taken

$$\delta\underline{q}_M = [\underline{L}_n \quad \underline{L}_c] \begin{bmatrix} \delta\underline{q}_n^{\text{ext}} \\ \delta\underline{q}_c^{\text{ext}} \end{bmatrix}. \tag{26}$$

Considering the system of equations in a converged micro energy balance state [20], the variations $\delta\underline{q}_n^{\text{ext}}$ and $\delta\underline{q}_c^{\text{ext}}$ can be extracted as,

$$\begin{bmatrix} \delta\underline{q}_n^{\text{ext}} \\ \delta\underline{q}_c^{\text{ext}} \end{bmatrix} = \begin{bmatrix} -\underline{T}^T\underline{K}_{ee}\underline{G} \\ -\underline{K}_{ce}\underline{G} \end{bmatrix} \delta\underline{\Upsilon}_M, \tag{27}$$

where the variations of the macroscopic quantities (loading terms) are involved. Using this relation in Eq. (26) finally yields the macroscopic tangent conductivity as

$$\underline{K}_M = (-\underline{L}_n\underline{T}^T\underline{K}_{ee}\underline{G} - \underline{L}_c\underline{K}_{ce}\underline{G}). \tag{28}$$

5.2.4. RVE–BVP coupled to the macroscopic mechanical pass

On an updated micro-domain (RVE at t_n passed to micro level in the macroscopic mechanical pass, see Table 1), the system is excited by the periodically microfluctuating displacement boundary conditions (see Eqs. (9a) and (9b)) which can be expressed in a constraint form as

$$\vec{x}_R = \vec{x}_L + \vec{x}_2 - \vec{x}_1, \tag{29a}$$

$$\vec{x}_T = \vec{x}_B + \vec{x}_4 - \vec{x}_1, \tag{29b}$$

where $\vec{x}_L$, $\vec{x}_R$, $\vec{x}_B$ and $\vec{x}_T$ denote current position vectors of the periodic points of the corresponding boundaries and $\vec{x}_i$, $i = 1, 2, 4$ are the position vectors of the corner nodes 1, 2 and 4 (see Fig. 2). Furthermore, with the updated temperature and temperature gradient calculated at each macroscopic integration point, the periodically microfluctuating temperature profile is enforced within the micro-domain as explained in Section 5.2.1. The resulting thermo-mechanical problem is solved in a staggered way.

The discretization of the weak form of the microscopic equilibrium equation yields a system of (non-)linear algebraic equations in the nodal displacements $\underline{u}$ which can be written as

$$\underline{f}_{\text{int}}(\underline{u}) = \underline{f}_{\text{ext}} \tag{30}$$

with $\underline{f}_{\text{int}}$ and $\underline{f}_{\text{ext}}$, the internal and external nodal forces, respectively. Linearization leads to the system of equations, as expressed in Eqs. (14a) and (15a), written in a compact form as

$$\underline{K}\delta\underline{u} = \delta\underline{r}, \tag{31}$$

where $\delta\underline{r}$ is the column with the out of balance residual forces. As a result of the periodically microfluctuating displacement boundary conditions, the displacement vectors of the corner nodes 1, 2 and 4 are kinematically fully prescribed by,

$$\vec{u}_i = (\boldsymbol{F}_M - \boldsymbol{I}) \cdot \vec{X}_i, \tag{32}$$

where the node corresponding to corner 1 is fixed to eliminate rigid body translations. The displacement of the node located at corner 3 is fully described by the displacement of corner 2 and corner 4. Therefore it is not an independent quantity anymore and consequently does not appear in the equations. Furthermore, as emphasized in the macroscopic thermal pass, the discretization of opposite sides of the RVE matches geometrically.

In the discrete setting, periodically microfluctuating displacement boundary conditions are handled through standard linear dependencies, $\delta\underline{u}_d = \underline{C}_{di}\delta\underline{u}_i$ with $\underline{u}_i$ the independent displacement degrees of freedom (dofs) and $\underline{u}_d$ the dependent dofs, mutually linked through the linear dependency matrix $\underline{C}_{di}$. Eliminating the dependent dofs from Eq. (31) leads to a condensed system

$$\underline{K}^*\delta\underline{u}_i = \delta\underline{r}^*, \tag{33}$$

which is further decomposed to account for the different contributions emanating from the macroscopically prescribed dofs, $\delta\underline{u}_p$ and the remaining free dof variations, $\delta\underline{u}_f$. At equilibrium of the RVE, this partitioned system reads

$$\begin{bmatrix} \underline{K}^*_{pp} & \underline{K}^*_{pf} \\ \underline{K}^*_{fp} & \underline{K}^*_{ff} \end{bmatrix} \begin{bmatrix} \delta\underline{u}_p \\ \delta\underline{u}_f \end{bmatrix} = \begin{bmatrix} \delta\underline{f}^*_p \\ \underline{0} \end{bmatrix}, \tag{34}$$

where $\delta\underline{f}^*_p$ corresponds to the variations of the external forces at the prescribed nodes. By condensing out the free degrees of freedom from the system, a reduced stiffness matrix linking $\delta\underline{f}^*_p$ and $\delta\underline{u}_p$ can be obtained as,

$$\underline{K}^*_{\mathrm{M}}\delta\underline{u}_p = \delta\underline{f}^*_p \quad \text{with} \quad \underline{K}^*_{\mathrm{M}} = \underline{K}^*_{pp} - \underline{K}^*_{pf}(\underline{K}^*_{ff})^{-1}\underline{K}^*_{fp}, \tag{35}$$

which will be used for the extraction of the macroscopic material tangent.

5.2.5. Extraction of the macroscopic stresses

The volume average of the microscopic first PK stresses can be converted into the following integral form:

$$\boldsymbol{P}_{\mathrm{M}} = \frac{1}{V_0}\int_{\Gamma_0} \vec{p}\vec{X}\,\mathrm{d}\Gamma_0 \tag{36}$$

for which the microscopic equilibrium and the identity $\vec{\nabla}_0\vec{X} = \boldsymbol{I}$ are used and $\vec{p}$ is defined as $\vec{p} = \boldsymbol{P}_{\mathrm{m}}\cdot\vec{N}$, where $\vec{N}$ is the unit outward normal to Γ_0, [16]. After the solution of the micro BVP, it can be verified that, in case of periodically microfluctuating displacement boundary conditions, the boundary integral (Eq. (36)) takes the following simple form:

$$\boldsymbol{P}_{\mathrm{M}} = \frac{1}{V_0}\sum_{i=1,2,4}\vec{f}_i\vec{X}_i, \tag{37}$$

where $\vec{f}_i$, $i = 1,2,4$ are the external forces at the three prescribed corner nodes, [16]. The macroscopic Cauchy stresses can be obtained from $\boldsymbol{P}_{\mathrm{M}}$ by a classical push-forward $\boldsymbol{\sigma}_{\mathrm{M}} = \frac{1}{\det\boldsymbol{F}_{\mathrm{M}}}\boldsymbol{P}_{\mathrm{M}}\cdot\boldsymbol{F}^{\mathrm{T}}_{\mathrm{M}}$.

5.2.6. Extraction of the macroscopic stiffness

For a constitutive relation formulated in the conjugate pair $\boldsymbol{P}$ and $\boldsymbol{F}$, the material tangent is the fourth order tensor $\mathbb{A}$ which satisfies the linear relation,

$$\delta\boldsymbol{P} = \mathbb{A}_{\mathrm{M}} : \delta\boldsymbol{F}. \tag{38}$$

Reconsidering Eq. (37), in a variational format,

$$\delta\boldsymbol{P}_{\mathrm{M}} = \frac{1}{V_0}\sum_{i=1,2,4}\delta\vec{f}_i\vec{X}_i \tag{39}$$

in combination with the expression for $\delta\underline{f}^*_p$ (see Eq. (35)) and $\delta\vec{u}_j = \delta\boldsymbol{F}_{\mathrm{M}}\cdot\vec{X}_j$, with $j = 1,2,4$ leads to the consistent tangent operator $\mathbb{A}_{\mathrm{M}}$ (see [13,16] for the derivation) according to

$$\mathbb{A}_{\mathrm{M}} = \frac{1}{V_0}\sum_i\sum_j(\vec{X}_i\underline{K}^{*(ij)}_{\mathrm{M}}\vec{X}_j)^{\mathrm{LC}} \quad i,j = 1,2,4 \tag{40}$$

where the left conjugation implies, $T^{\mathrm{LC}}_{ijkl} = T_{jikl}$. $\underline{K}^*_{\mathrm{M}}$ is a 6×6 matrix for a 2-D RVE configuration and $\underline{K}^{*(ij)}_{\mathrm{M}}$ is a square sub-matrix of $\underline{K}^*_{\mathrm{M}}$ corresponding to the dofs of the nodes i and j $(i,j = 1,2,4)$.

Once $\mathbb{A}_{\mathrm{M}}$ is obtained, the required material tangent in an updated Lagrangian framework can be derived through a push-forward (see [31]) written in index notation as

$$C_{pqmn} = F_{qJ}A_{pJmS}F_{nS} - J\delta_{mp}\sigma_{nq}, \tag{41}$$

where C_{pqmn} is the material tangent consistent with Eq. (15a), $J = \det\boldsymbol{F}_{\mathrm{M}}$ and δ_{mp} is the Kronecker delta.

6. Two-scale homogenization examples

The proposed two-scale thermo-mechanical framework has been implemented in a commercial FE environment (MSC MARC), and is next demonstrated by two example problems. The selected problems are 2-D, preferred due to computational cost reasons, although the presented framework is applicable to 3-D cases as well.

6.1. Thermo-mechanically loaded plate

In Fig. 3, a long plate, made of boron fiber reinforced aluminum is shown. The fibers are unidirectionally oriented parallel to the z-axis. The plate is clamped on its side surfaces and exposed to a rapidly increasing uniform temperature and mechanical load on the top surface. The final temperature of 250 °C is reached in 10 s (in 50 steps) on the top surface whereas the temperature at the bottom surface is kept constant at $T_0 = 20$ °C. The uniformly distributed mechanical load has a final value of 100 N/m^2, which is reached in 10 s as well. The problem can be idealized as a plane strain problem (no deformation in z-direction) and due to symmetry, only one half of the plate is modeled with 120 eight-noded elements with a reduced integration scheme. The boundary conditions and the dimensions are sketched in Fig. 3. It is assumed that the geometrical pattern of the fibers is regular so that the underlying microstructure can be fully described by a two-phase unit cell visualized in Fig. 3, which serves as the representative volume element (RVE) for the microstructural computations.

Mechanically, the boron fibers are linearly elastic with a modulus of elasticity E = 385 GPa, Poissons' ratio $\nu = 0.2$, and a coefficient of thermal expansion $\alpha = 5.0\ 10^{-6}$/°C. The aluminum matrix is taken to be elasto-plastic with isotropic hardening. The corresponding mechanical parameters for the matrix are, E = 75 GPa, $\nu = 0.33$, $\alpha = 2.36\ 10^{-5}$/°C, with a yield stress σ_y = 300 MPa and a hardening modulus h = 150 MPa. Thermally, both constituents are described by Fourier's law with the temperature independent material data for the fibers, given by their conductivity $\lambda = 38$ W/mK and their heat capacity, $c_\upsilon = 1.3$ kJ/kg K. The corresponding material data set for the matrix is, λ = 247 W/mK and $c_\upsilon = 0.9\ kJ/kgK$. The densities used for the heat storage capacity calculations are $\rho = 2600$ kg/m^3 for the fibers and ρ = 2700 kg/m^3 for the matrix, respectively. At the RVE level, four-noded quadrilaterals with a constant dilatation formulation are used for the discretization. A convergence criterion which compares the maximum residual and maximum reaction forces, is used at the RVE level and the ratio is forced to be smaller than 10^{-8}, in order to obtain accurate results for quantities to be transferred to the macro level. The same convergence criterion with a threshold of 10^{-3} is used at the macro level.

For comparison purposes, the same problem is analyzed with a Taylor approach and a modified Sachs approach. Basically, the Taylor approach assumes that: (I) mechanically both phases experience the same deformation and (II) thermally the same temperature gradient is effective within each phase. Therefore, traction and heat flux continuity across the fiber matrix interface will be violated. On the other hand, the classical Sachs approach enforces that

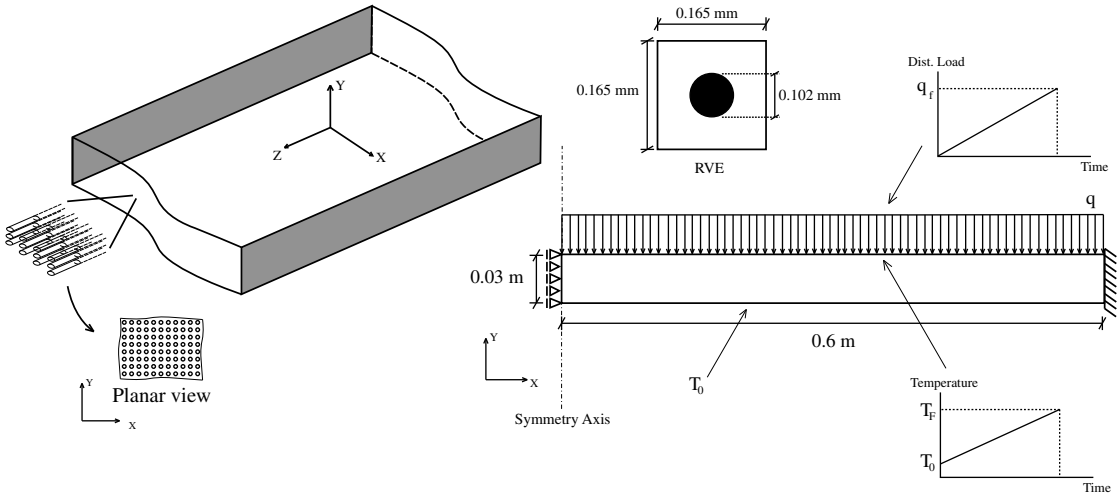

Fig. 3. Thermo-mechanically loaded plate; geometry, boundary conditions and RVE.

stresses and fluxes are same in both phases while the 'macroscopic' displacement gradient and the temperature gradient are assumed to be the weighted sum (by volume fractions) over the two phases. Here a slight modification is introduced assuming that the rotation tensors in both phases are identical. It is noteworthy to mention that most relatively simple and more accurate alternative methods [32,33] are applicable only in a uni-axial stress/strain state.

In Fig. 4, the deformed configuration of the plate with the resulting von Mises stresses is presented and two RVE's which are located at the integration points A and B are depicted. Both the mechanical and thermal fields are shown. From the plastic strain distribution at the micro level, it can be concluded that the matrix experiences severe yielding particularly at the locations of large curvature (e.g., integration point A). The resulting homogenized macroscopic response is plotted in Fig. 5. The horizontal reaction force and the bending moment per unit length in z-direction developing at the mid-section (symmetry axis) are presented graphically. On the horizontal axis, the vertical displacement of the mid-section is given (through the thickness, the variations of the vertical displacements are negligible). The responses obtained through the Taylor assumption and modified Sachs approach are also depicted. For the Taylor solution, (where both phases experi-

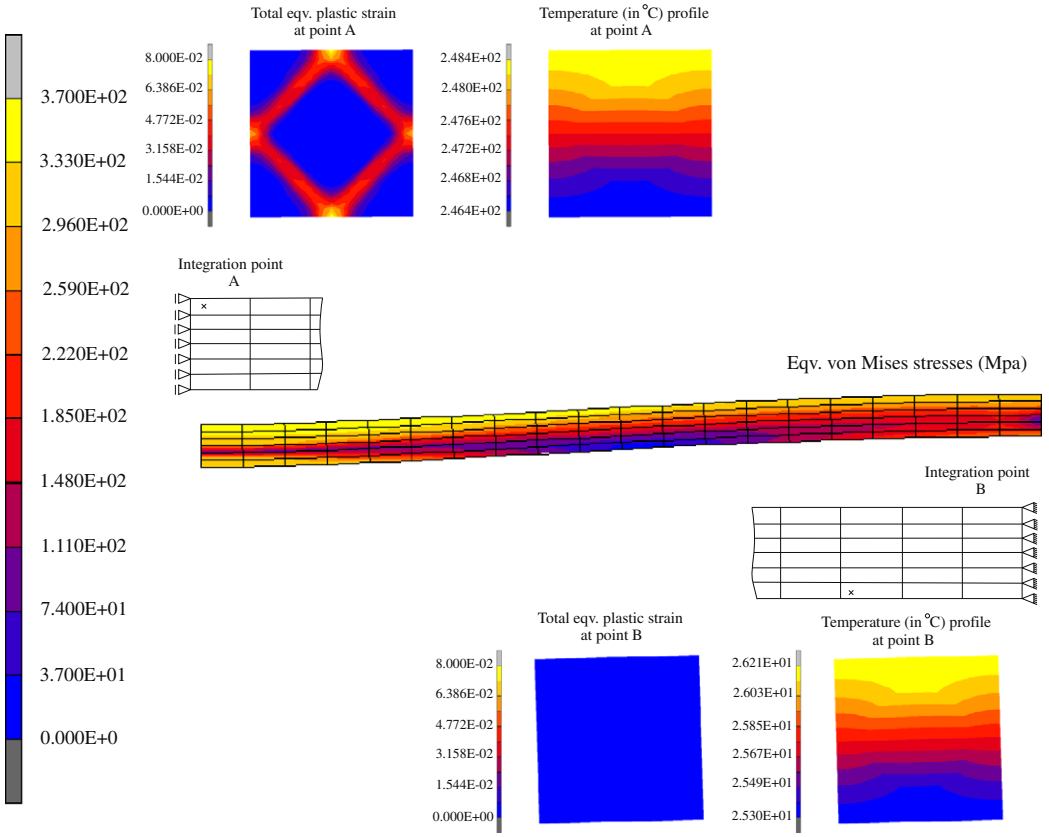

Fig. 4. Two-scale solution via computational homogenization at $t = 10.0$ s.

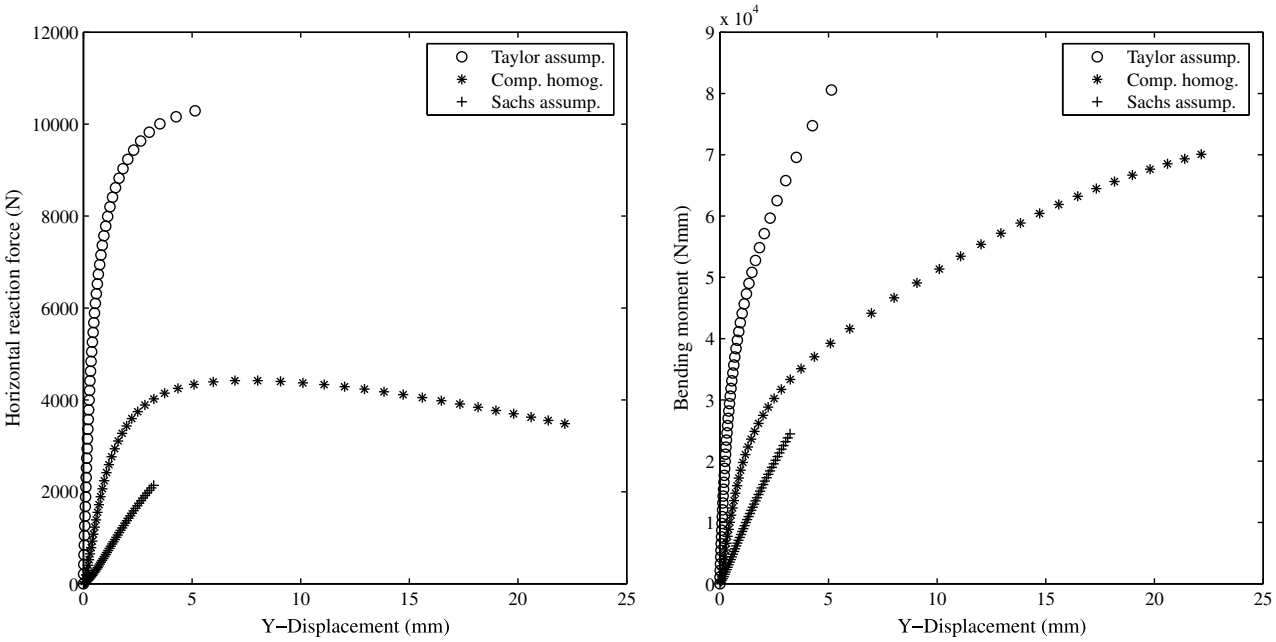

Fig. 5. Horizontal reaction force and bending moment at the mid-section (sym. axis).

ence the same deformation) the relatively stiff fiber contributes excessively to the cross-sectional resistance which leads to high axial and bending stiffnesses, reflecting the well-known Taylor upper bound. The Sachs assumption leads to a very compliant structure which does not show any yielding with a smaller axial force and bending moments, typically associated with the lower bound. As expected, the computational homogenization scheme provides a solution in between these two bounds, yet obviously substantially different.

Furthermore, to assess the chosen time step size, the problem is solved for four different step sizes which has yielded 25, 50, 100 and 200 steps. The vertical displacement of the mid-section for four different cases is presented in Fig. 6 which clearly shows the convergence of the displacement. Furthermore, the graph also indicates that the chosen step size is sufficiently small to avoid instabilities.

6.2. Thermally shocked channel

In the second example, the thermo-mechanical analysis focuses on a long channel, which is typically used for hot molten metal transport as shown in Fig. 7. Due to symmetry and the high channel length, the problem is idealized as a plane strain problem of the half-width channel for which the corresponding dimensions and boundary conditions are sketched in the figure. The channel is exposed to a temperature shock at the inner surface which reaches a final temperature T_F of 500 °C in 4 s starting from an initial temperature T_0 of 20 °C. The outer surface is kept at its initial temperature level throughout the entire loading history.

Due to its high temperature resistance, an alumina based refractory ceramic is typically used for this type of structures. The underlying microstructure is of a granular type with directionally distinct characteristics resulting from the raw base materials and

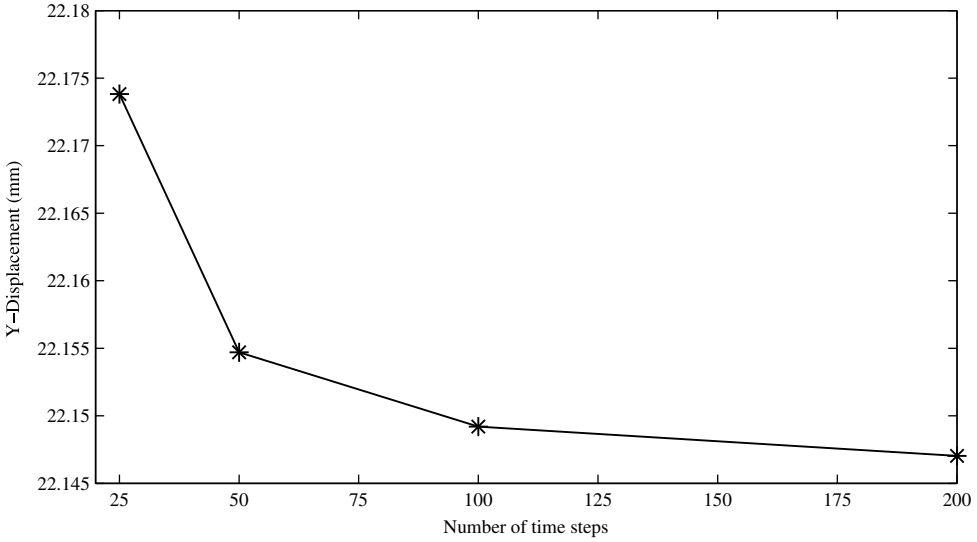

Fig. 6. Vertical displacement at the mid-section (sym. axis) vs. number of time steps.

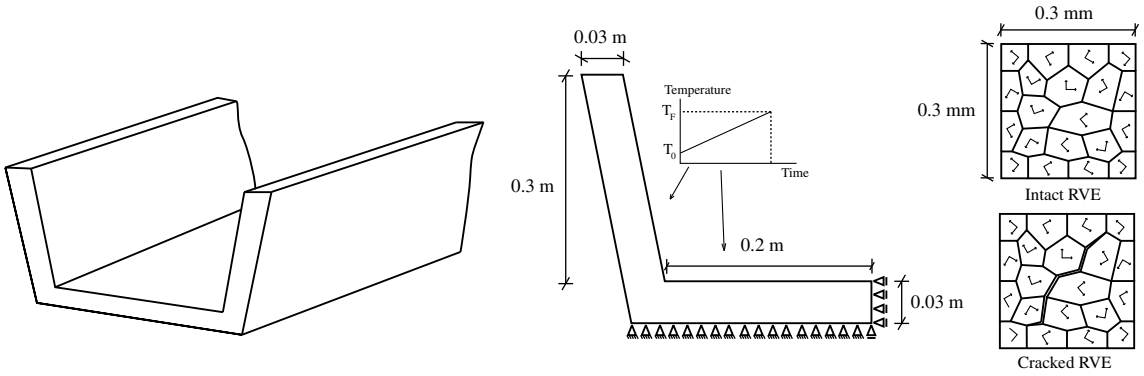

Fig. 7. Channel exposed to thermal shock; geometry, boundary conditions and RVE's.

the production process. The RVE's used for the microstructural representation are also shown in Fig. 7. To investigate the effect of prior damage on the thermo-mechanical response, an 'intact RVE' as well as a diagonally cracked RVE are considered. The crack in the latter is modeled by assuming a locally degenerated mechanical stiffness and thermal properties of air within the crack domain. Both mechanically and thermally, it is assumed that individual grains at the RVE level have an anisotropic behaviour. The principal directions of anisotropy are differently oriented from grain to grain as indicated in Fig. 7.

Based on the crystal structure (tetragonal) of alumina [34], anisotropic mechanical constants equal to $c_{11} = 465\ GPa$, $c_{22} = 465$ GPa, $c_{33} = 563$ GPa, $c_{12} = 124$ GPa, $c_{13} = 117$ GPa, $c_{44} = 233$ GPa are used [35]. The principal values of the conductivity tensor are 38 W/mK and 10 W/mK. Heat capacity and the density are taken to be $c_v = 120$ J/kg K and $\rho = 2700$ kg/m^3, respectively. The principal directions of the grains are distributed randomly.

Both at micro and macro level, the same convergence norms as used in the first problem are employed. In Fig. 8, the resulting von Mises stresses obtained at the end of the loading history are visualized. As seen from the contour plot, the maximum stress values are reached on the horizontal part of the channel and the inclined part experiences limited stresses due to the lack of boundary constraints there. On the right-hand side of Fig. 8, the temperature and the equivalent von Mises stresses in a typical cross-sections are presented. The difference between the maximum stresses obtained by the rule of mixture (which is presented for comparison purposes) and the computational homogenization is about 30% which would make a significant difference for crack initiation predictions. The difference between the two solutions for the temperature profile reaches about 10% at the centre of the cross-section which remains significant.

To investigate qualitatively the effect of thermo-mechanical damage (i.e. disconnected grains) e.g. due to abrupt temperature changes and cycles, the equivalent macroscopic response is also predicted using the RVE with prior damage (see Fig. 7).

On the left-hand side of Fig. 9, the macroscopic response for the pre-damaged RVE is presented including two RVE stress distributions located at the indicated cross-sections (integration points closest to the inner surface). Mechanically, the crack leads to a more flexible response which results in larger displacements.

On the right-hand side of Fig. 9, the microscopic von Mises stresses and the temperature profiles of the intact and pre-damaged RVE's, which are located at the same macroscopic position,

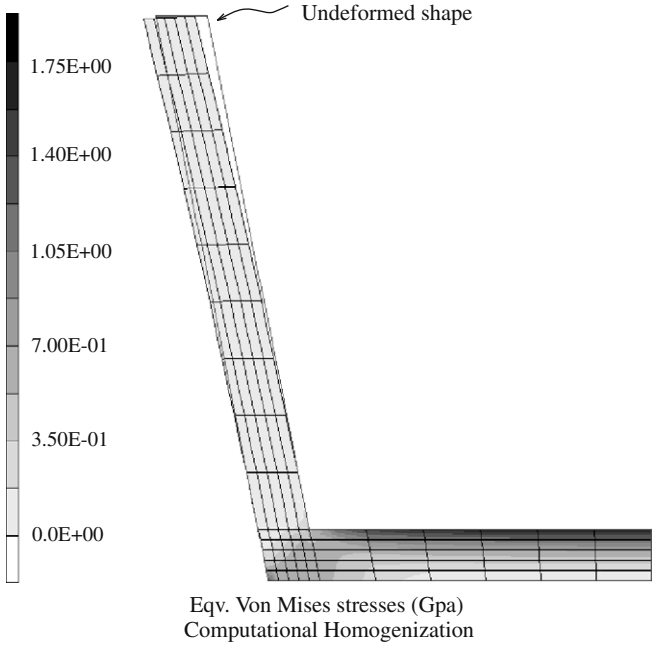

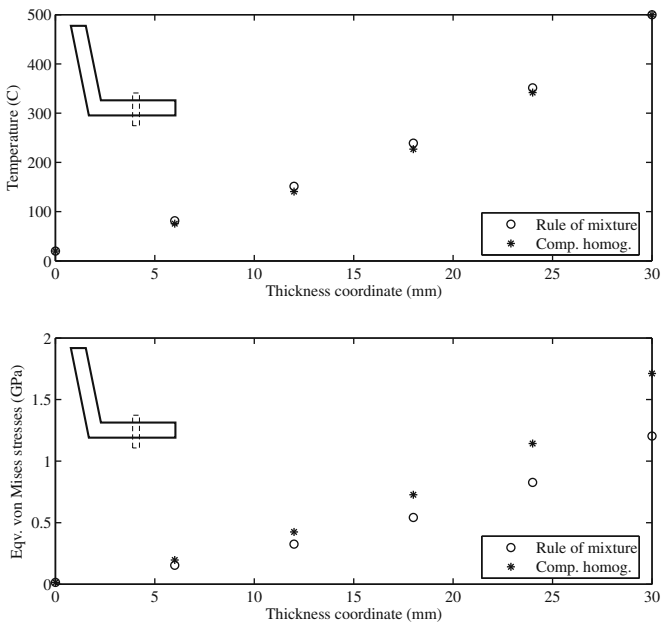

Fig. 8. Equivalent von Mises stresses and temperature profile in a typical cross-section.

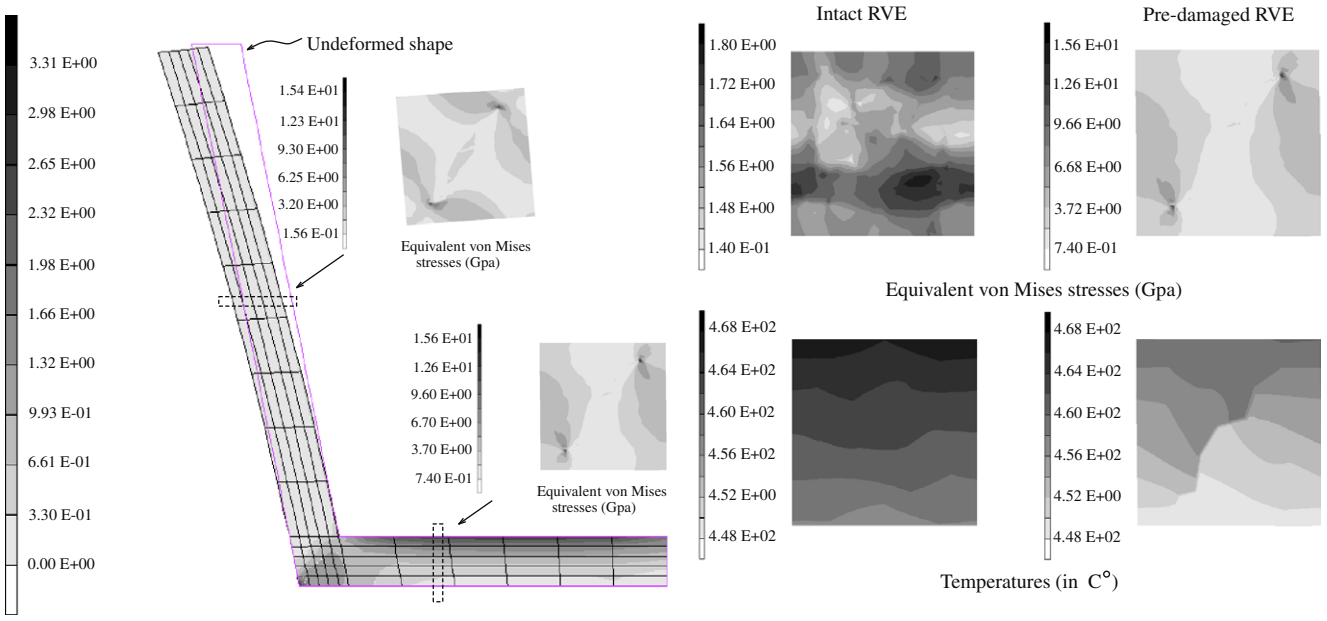

Fig. 9. Equivalent von Mises stresses and micro-scale response for intact and damaged RVE's.

are depicted. Obviously, the crack leads to a significant change in the thermal and mechanical response, both qualitatively and quantitatively.

7. Summary and conclusion

Motivated by the results obtained in [13,15,20], a two-scale analysis framework for the thermo-mechanical analysis of heterogeneous solids has been presented. Thermo-mechanical approaches at both scales are treated consistently and linked by a rigorous scale bridging procedure. Using an extended computational homogenization framework, macroscopic thermal and mechanical excitations are passed to the micro level through appropriate RVE boundary conditions. The resulting microscopic response is homogenized to the macro-scale by means of consistent averaging relations. Tangent operators for a coupled FE^2 solution strategy are derived in a consistent manner. An operator-split implementation has been elaborated, separating thermal and mechanical passes. As demonstrated by the example problems, the method resolves the interaction between the mechanical and thermal fields at the micro level, accounting for temperature dependent microscopic properties. Both coarse scale and fine scale results are revealed, providing insight on the structural level and the material level in a simultaneous manner. Original aspects and the added values of the proposed approach are:

- A rigorous method for the thermo-mechanical analysis of heterogeneous solids has been developed, which does not require explicit macroscopic (homogenized) quantities such as an effective thermal expansion coefficient.
- Anisotropy, non-linearity and temperature dependence of both mechanical and thermal material characteristics can be introduced at the micro level with various morphologies enabling an effective structure–property analysis. Classical homogenization techniques are inadequate in this context if temperature dependent and mechanically non-linear micro-phase properties have to be resolved.
- The interaction between the thermal and mechanical fields is tackled at the micro level and the proposed algorithmic framework has the potential to include further interactions which may result from microstructural evolution (e.g. thermo-mechanical damage and debonding). Failure mechanisms induce a strong coupling between micro and macro scales for which this approach is undoubtedly beneficial.
- Results obtained through the proposed methodology may serve as a reference for alternative simplified homogenization schemes.

For typical high temperature resistant materials, the failure cannot really be qualified as perfectly brittle, however, the microstructural evolution can be modeled by the use of cohesive zones along the interfaces and diffusive thermo-mechanical damage within different phases. In combination with these techniques, the proposed method can be used to investigate the effect of microstructural variables (both geometrical and physical) on the macroscopic failure initiation including the relation to the underlying thermal and mechanical microstructural evolution. This allows to enhance the understanding and modeling of failure and clarifies the active field interaction effects. These insights cannot be extracted from a single scale phenomenological modeling approach.

References

[1] Z. Hashin, The elastic moduli of heterogeneous materials, J. Appl. Mech. 29 (1962) 143–150.
[2] B.W. Rosen, Z. Hashin, Effective thermal expansion coefficients and specific heats of composite materials, Int. J. Engrg. Sci. 8 (1970) 157–173.
[3] J.M. Guedes, N. Kikuchi, Preprocessing and postprocessing for materials based on the homogenization method with adaptive finite element methods, Comput. Methods Appl. Mech. Engrg. 83 (1990) 143–198.
[4] P.W. Chung, K.K. Tamma, Homogenization of temperature-dependent thermal conductivity in composite materials, AIAA J. Thermophysics Heat Transfer 15 (1) (2001) 10–17.
[5] P.W. Chung, K.K. Tamma, Woven fabric composites – developments in engineering bounds, homogenization and applications, Int. J. Numer. Methods Engrg. 45 (1999) 1757–1790.
[6] D. Golanski, K. Terada, N. Kikuchi, Macro and micro scale modeling of thermal residual stresses in metal matrix composite surface layers by the homogenization method, Comput. Mech. 19 (1997) 188–202.
[7] S. Ghosh, Y. Liu, Voronoi cell finite element model based on micropolar theory of thermoelasticity for heterogeneous materials, Int. J. Numer. Methods Engrg. 38 (1995) 1361–1398.
[8] S. Moorthy, S. Ghosh, Y.S. Liu, Voronoi cell finite element model for thermo-elastoplastic deformation in random heterogeneous media, Appl. Mech. Rev. 47 (1) (2001) 207–221.

[9] J. Fish, K.L. Shek, Finite deformation plasticity of composite structures: Computational models and adaptive strategies, Comput. Methods Appl. Mech. Engrg. 172 (1999) 145–174.
[10] J. Fish, Q. Yu, Multiscale damage modeling for composite materials: theory and computational framework, Int. J. Numer. Methods Engrg. 52 (2001) 161–192.
[11] R.J.M. Smit, W.A.M. Brekelmans, H.E.H. Meijer, Prediction of the mechanical behaviour of non-linear heterogeneous systems by multi-level finite element modeling, Comput. Methods Appl. Mech. Engrg. 155 (1998) 181–192.
[12] F. Feyel, J.L. Chaboche, FE^2 multiscale approach for modeling the elastoviscoplastic behaviour of long fibre Sic/Ti composite materials, Comput. Methods Appl. Mech. Engrg. 183 (2000) 309–330.
[13] V.G. Kouznetsova, W.A.M. Brekelmans, F.P.T. Baaijens, An approach to micro–macro modeling of heterogeneous materials, Comput. Mech. 27 (2001) 37–48.
[14] C. Miehe, J. Schröder, J. Schotte, Computational homogenization analysis in finite plasticity. Simulation of texture development in polycrystalline materials, Comput. Methods Appl. Mech. Engrg. 171 (1999) 387–418.
[15] V.G. Kouznetsova, M.G.D. Geers, W.A.M. Brekelmans, Multi-scale constitutive modelling of heterogeneous materials with a gradient-enhanced computational homogenization scheme, Int. J. Numer. Methods Engrg. 54 (2002) 1235–1260.
[16] V.G. Kouznetsova, Computational homogenization for the multi-scale analysis of multi-phase materials, Ph.D. thesis, Eindhoven University of Technology, 2002. <http://www.mate.tue.nl/mate/publications/index.php/4/2002>.
[17] T.J. Massart, R.H.J. Peerlings, M.G.D. Geers, Structural damage analysis of masonary walls using computational homogenisation, Int. J. Damage Mech. 16 (2007) 199–226.
[18] M.G.D. Geers, E. Coenen, V.G. Kouznetsova, Multi-scale computational homogenization of structured thin sheets, Model. Simulat. Mater. Sci. Engrg. 15 (2007) S393–S404.
[19] K. Matouš, M.G. Kulkarni, P.H. Geubelle, Multiscale cohesive failure modeling of heterogeneous adhesives, J. Mech. Phys. Solids 56 (4) (2008) 1511–1533.
[20] I. Özdemir, W.A.M. Brekelmans, M.G.D. Geers, Computational homogenization for heat conduction in heterogeneous solids, Int. J. Numer. Methods Engrg. 73 (2) (2008) 185–204.
[21] S. Nemat-Nasser, M. Hori, Micromechanics: overall properties of heterogeneous solids, North-Holland Series in Applied Mathematics and Mechanics, North-Holland, 1993.
[22] T. Kanit, S. Forest, I. Galliet, V. Mounoury, D. Jeulin, Determination of the size of the representative volume element for random composites: statistical and numerical approach, Int. J. Solids Struct. 40 (2003) 3647–3679.
[23] J. Zeman, M. Šejnoha, Numerical evaluation of effective elastic properties of graphite fiber tow impregnated by polymer matrix, J. Mech. Phys. Solids 49 (1) (2001) 69–90.
[24] O. van der Sluis, P.J.G. Schreurs, W.A.M. Brekelmans, H.E.H. Meijer, Overall behaviour of heterogeneous elastoviscoplastic materials: effect of microstructure modelling, Mech. Mater. 32 (2000) 449–462.
[25] V.G. Kouznetsova, M.G.D. Geers, W.A.M. Brekelmans, Multi-scale second-order computational homogenization of multi-phase materials: a nested finite element solution strategy, Comput. Methods Appl. Mech. Engrg. 193 (2004) 5525–5550.
[26] H.W. Zhang, S. Zhang, J.Y. Bi, B.A. Schrefler, Thermo-mechanical analysis of periodic multiphase materials by a multiscale asymptotic homogenization approach, Int. J. Numer. Methods Engrg. 69 (2007) 87–113.
[27] J.L. Auriault, Effective macroscopic description of heat conduction in periodic composites, Int. J. Heat Mass Transfer 26 (6) (1983) 861–869.
[28] M. Ostoja-Starzewski, Towards stochastic continuum thermodynamics, J. Non-equilibrium Thermodyn. 27 (2002) 335–348.
[29] R.M. McMeeking, J.R. Rice, Finite element formulations for large elastic–plastic deformations, Int. J. Solids Struct. 11 (1975) 601–616.
[30] J. Bonet, R.D. Wood, Nonlinear Continuum Mechanics for Finite Element Analysis, Cambridge University Press, 1997.
[31] J.C. Simo, J.T. Hughes, Computational Inelasticity Interdisciplinary Applied Mathematics, Springer-Verlag, 2000.
[32] T.S. Byun, I.S. Kim, Stress and strain partition in elastic and plastic deformation of two phase alloys, J. Mater. Sci. 26 (1991) 3917–3925.
[33] O. Bouaziz, P. Buessler, Iso-work increment assumption for heterogeneous material behaviour, Adv. Engrg. Mater. 6 (2004) 79–83.
[34] J.F. Nye, Physical Properties of Crystals, Oxford University Press, Oxford, 1985.
[35] M. Swain (Ed.), Structure and Properties of Ceramics Materials Science and Technology, vol. 11, VCH, 1994.